



# Experimental Characterization of the Resistance of Tubular Aluminum Sections <sup>†</sup>

Sahar Dahboul <sup>1</sup> , Liya Li <sup>2</sup>, Prachi Verma <sup>1</sup>, Pampa Dey <sup>1</sup> and Nicolas Boissonnade <sup>1,\*</sup> 

<sup>1</sup> Department of Civil and Water Engineering, Laval University, Quebec City, QC G1V0A7, Canada; sahar.dahboul.1@ulaval.ca (S.D.); prachi.verma.1@ulaval.ca (P.V.); pampa.dey@gci.ulaval.ca (P.D.)

<sup>2</sup> Department of Civil and Building Engineering, Université de Sherbrooke, Québec, QC J1K 2R1, Canada; liya.li@usherbrooke.ca

\* Correspondence: nicolas.boissonnade@gci.ulaval.ca

<sup>†</sup> Presented at the 15th International Aluminium Conference, Québec, QC, Canada, 11–13 October 2023.

**Abstract:** Aluminum has a bright future as a structural material due to its excellent corrosion resistance, durability, lightweight, and complete recyclability. However, it is necessary to fully understand its mechanical behaviour under various loading conditions to make it competitive with other materials, such as concrete or steel, for civil engineering applications, especially as primary load-bearing structural members. To develop an in-depth knowledge on the behaviour of extruded aluminum sections of various shapes, an extensive experimental study was undertaken with specific emphasis on analyzing the buckling response of rectangular and square hollow sections (RHS and SHS) with 6061-T6 aluminum alloy under compressive loads. In this regard, six stub column tests were performed under axial compression, while eleven short beam-column tests under eccentric compression are currently in progress. Additionally, six tensile coupon tests were performed to obtain the full material stress–strain curve, and initial geometrical imperfections were measured mechanically and using a 3D scanner. Finally, the results of the stub column tests were compared to the resistances calculated using the Canadian standard CSA S157, which were generally conservative compared to the experimental observations.

**Keywords:** aluminum alloy; RHS and SHS; experimental tests; local buckling



**Citation:** Dahboul, S.; Li, L.; Verma, P.; Dey, P.; Boissonnade, N. Experimental Characterization of the Resistance of Tubular Aluminum Sections. *Eng. Proc.* **2023**, *43*, 19. <https://doi.org/10.3390/engproc2023043019>

Academic Editor: Mario Fafard

Published: 14 September 2023



**Copyright:** © 2023 by the authors. Licensee MDPI, Basel, Switzerland. This article is an open access article distributed under the terms and conditions of the Creative Commons Attribution (CC BY) license (<https://creativecommons.org/licenses/by/4.0/>).

## 1. Introduction

In recent years, aluminum alloys have received significant structural interest due to their unique properties and potential benefits. These alloys present many benefits, encompassing great corrosion resistance, a high strength-to-weight ratio, excellent durability, and full recyclability [1–3]. However, despite these notable attributes, aluminum alloys have yet to establish themselves as a reliable alternative to conventional structural materials like concrete and steel. This is primarily attributed to the lower Young’s modulus of aluminum alloys, which is approximately one-third of that of carbon steel. Consequently, this inherent characteristic can adversely affect the buckling behaviour and stiffness of aluminum structural components. However, investigating these phenomena remains an area that requires further research and investigations.

In the past, many researchers conducted series of experimental studies to examine the load-carrying capacity of aluminum structural members and investigate their local and global buckling behaviours. These investigations encompassed various cross-sectional profiles, including hollow sections [4–12], U-shapes [4], angles [13,14], and I-shapes [8,15]. However, it is noteworthy that the majority of these studies primarily concentrated on the buckling behaviour of sections subjected to axial compression, with relatively limited emphasis on the buckling response under eccentric compression [16]. Hence, this study aims at carrying out a comprehensive experimental program at the “Laboratoire de génie civil” of the Laval University to investigate the ultimate carrying capacities and failure

modes of extruded aluminum hollow sections when subjected to both axial and eccentric compressions. In particular, the experimental study was designed for three different types of hollow sections, square hollow sections with sharp corners ( $RT6 \times 6 \times 0.5\text{-SC}$ ), square hollow sections with rounded corners ( $RT6 \times 6 \times 0.5\text{-RC}$ ), and rectangular hollow sections with sharp corners ( $RT6 \times 3 \times 3/16\text{-SC}$ ), which are popularly used in bridge infrastructures and for which buckling is often the governing design criteria.

To achieve the objective of this study, six tensile tests were carried out to accurately determine the material stress–strain behaviour. Furthermore, the initial geometrical imperfections of each specimen were carefully measured beforehand using mechanical techniques and 3D scanning technologies. To determine the ultimate capacity under axial compression, six stub column tests were undertaken, which were then compared with the predictions made by the Canadian standard. Ongoing experiments involve tests on 11 short beam-column specimens under eccentric compression. Altogether, the outcomes from these tests under axial and eccentric compressions will contribute to the development of new design rules for aluminum extrusions.

## 2. Preliminary Measurements

The experimental program involves preliminary measurements of geometric dimensions and imperfections that are crucial for the predictions of buckling resistance of aluminum extrusions. These measurements are also necessary to validate the numerical models of such sections that will be developed in the future course of this research. A description of each of these measurements is provided below.

### 2.1. Dimensions and Geometrical Imperfections

The actual geometrical dimensions of all specimens were measured using a digital caliper with an accuracy of 0.1 mm, including flange width  $b_{\text{Flange}}$ , web height  $h_{\text{Web}}$ , flange thickness  $t_{\text{Flange}}$ , web thickness  $t_{\text{Web}}$ , and specimen's length  $L$ . These measurements were repeated at the top, middle, bottom, and intermediate positions along the length of each specimen to obtain accurate measurements. The average measurements of the specimens are summarized in Table 1.

**Table 1.** Measured geometrical properties and imperfections of tested specimens.

Sections	$b_{\text{Flange}}$ [mm]	$h_{\text{Web}}$ [mm]	$t_{\text{Flange}}$ [mm]	$t_{\text{Web}}$ [mm]	L [mm]	wFlange [mm]	wWeb [mm]
RT6 × 6 × 0.5-SC-STUB1	152.91	152.795	13.065	13.095	399.45	0.176	0.174
RT6 × 6 × 0.5-SC-STUB2	152.735	152.885	12.795	12.705	400.15	0.164	0.149
RT6 × 6 × 0.5-RC-STUB1	152.985	153.425	12.765	13.13	398.55	0.228	0.150
RT6 × 6 × 0.5-RC-STUB2	152.95	153.33	12.815	13.09	398.48	0.307	0.081
RT6 × 3 × 3/16-SC-STUB1	76.05	151.94	4.505	4.5	398.62	0.255	0.356
RT6 × 3 × 3/16-SC-STUB2	76.07	152.05	4.52	4.475	398.75	0.194	0.426

Furthermore, a comprehensive analysis on the local geometrical imperfections of the tested specimens was conducted to better characterize the onset of local buckling and its influence on cross-sectional capacity. The measurements of local geometrical imperfections were meticulously carried out twice for all specimens using both mechanical techniques and a portable Metra SCAN 3D laser scanner [17]. The mechanical techniques involved placing a specimen on a milling bed machine, securely clamping it, and subsequently obtaining measurements of the geometrical imperfections utilizing a micrometer with an accuracy of 1 micron. This process is depicted in Figure 1a. In parallel, the second method employed a professional-grade Metra SCAN 3D scanner, renowned for its high precision, with the ability to measure the positions of scattered points accurately up to 0.025 mm [17]. The scanning procedure and the equipment employed in this method are presented in Figure 1b. The maximum measured magnitude of local imperfections for the flange (wFlange) and for the web (wWeb) are summarized in Table 1, which will be utilized to develop the numerical

models and investigate the effect of geometrical imperfections on the buckling behaviour of aluminum sections.

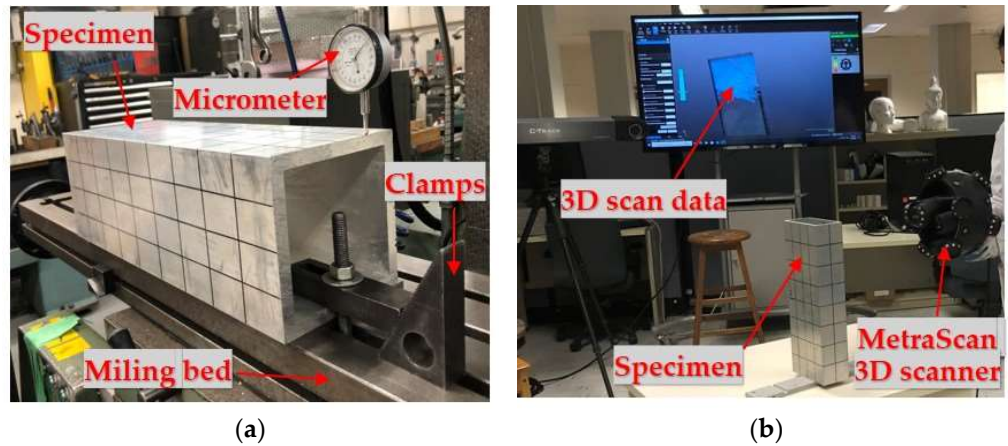


Figure 1. Geometrical imperfection measurements (a) by means of mechanical techniques, and (b) using MetraSCAN 3D scanner.

2.2. Tensile Coupon Tests

Tensile coupon tests were performed to accurately determine the material properties of 6061-T6 aluminum alloy for subsequent experimental analyses and for the development of finite element models. Two tensile coupons were selected from the upper flange (UF) and right web (RW) of each cross-sectional shape. These coupons were prepared carefully following the recommendations of the American Society for Testing and Materials (ASTM) standards [18] and of the EN ISO 377 standards [19]. The experimental setup, as depicted in Figure 2a, utilized an MTS 500 kN hydraulic testing machine operating under displacement control. A calibrated extensometer with a base length of 20 mm was fixed at the midpoint of each coupon to monitor the average longitudinal strain. The testing procedure and loading rate followed the recommended guidelines provided in [20], which involved several loading and unloading cycles for accurate determination of  $E$  and  $\sigma_{0.2}$ .

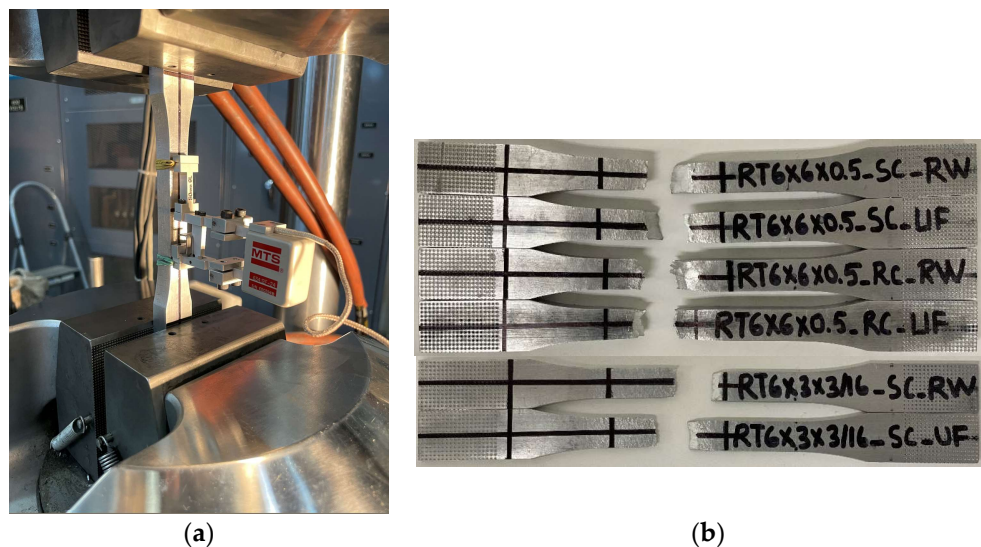


Figure 2. Tensile coupon tests: (a) test setup, and (b) coupons after fracture.

Figure 2b presents the coupons after failure. The key material properties obtained from the tensile tests are summarized in Table 2, which include the measured average initial Young’s modulus  $E_0$ , the 0.2% static tensile proof stress  $\sigma_{0.2}$ , the 1.0% proof stress  $\sigma_{1.0}$ , the ultimate tensile strength  $\sigma_u$ , the strain at the ultimate strength  $\epsilon_u$ , and the exponent

$n$  of the Ramberg–Osgood law. All these parameters obtained from the tensile coupon tests will help in validating the numerical models, which will be developed using the ABAQUS software as the future scope of this work.

**Table 2.** Material properties of tested specimens.

Sections	$E$ [MPa]	$\sigma_{0.2}$ [MPa]	$\sigma_{1.0}$ [MPa]	$\sigma_u$ [MPa]	$\epsilon_u$ [%]	$n$ [-]
RT6 × 6 × 0.5-SC-TENSILE	69,398	291.48	299.12	314.07	6.09	67
RT6 × 6 × 0.5-RC-TENSILE	70,130	293.50	300.50	308.90	6.06	46
RT6 × 3 × 3/16-SC-TENSILE	66,488	303.39	311.09	322.13	6.07	57
According to the Canadian Standard	70,000	240		260		55

### 3. Stub Column Tests

To investigate the behavior of the specimens under axial compression, a series of six stub column tests were conducted, with two tests being performed on each section shape. The repetition of two tests was to characterize the level of confidence in the experimental results. The nominal length of the stub columns was determined to be approximately three times the larger dimension of the cross-section, specifically the web height. This ensured that the effects of flexural buckling were avoided/minimized while providing a sufficient length to ensure a minimal influence of the end supports. Moreover, to achieve uniform distribution of compressive stresses during testing, meticulous attention was paid to grinding both ends of the specimens to ensure that they were flat and perpendicular to the longitudinal axis.

The compression tests were carried out using a high-capacity 5000 kN SATEC hydraulic machine, as illustrated in Figure 3. For an accurate recording of the end shortening response of the stub column during testing, an LVDT was positioned on the top end plate, while the bottom plate remained fixed. The stub column tests were conducted under displacement control, maintaining a constant rate of 0.15 mm/min for the rectangular hollow sections and 0.5 mm/min for the square hollow sections. This controlled testing approach allowed accurate and consistent data acquisition throughout the experiments.

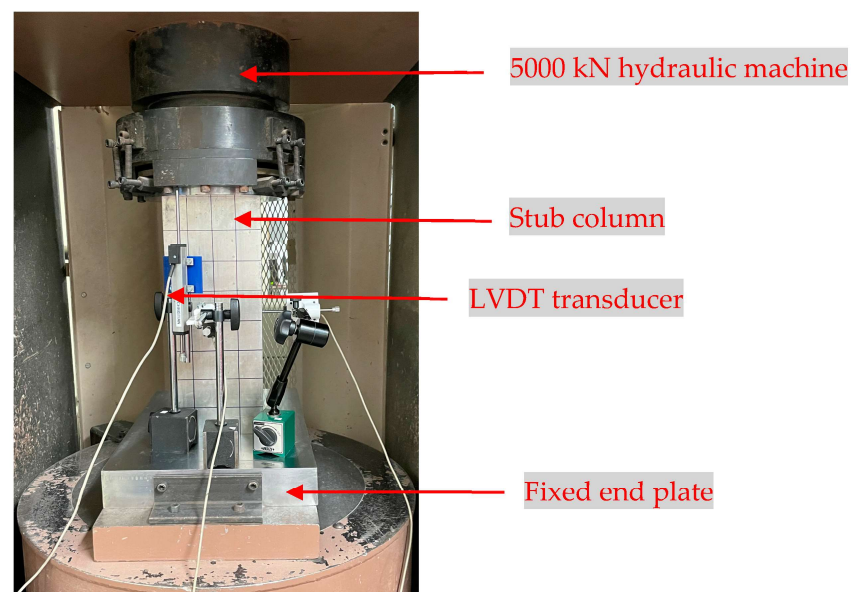


**Figure 3.** A representative picture of the test setup during the stub column tests.

The failure modes observed in the stub column tests are shown in Figure 4. All specimens exhibited pure local buckling as the primary mode of failure, without any coupling phenomena. Typical failure modes were observed for the rectangular hollow

sections and the square hollow sections with rounded corners. In these cases, both inward and outward buckling occurred across the plates, as shown in Figure 4a,b. In comparison, the square hollow sections with sharp corners exhibited only outward buckling, with no presence of inward deformation, as shown in Figure 4c. In addition, surface cracking was observed near the bottom of the specimens, which could be attributed to the thick and stocky plates. In addition, the sharp angles of these sections accentuated their stiffness, while the high level of deformation required for failure meant that the onset of fractures occurred well beyond the maximum load, making them less indicative of overall behaviour. These failure modes will be one of the response variables in validating the numerical models in the future.

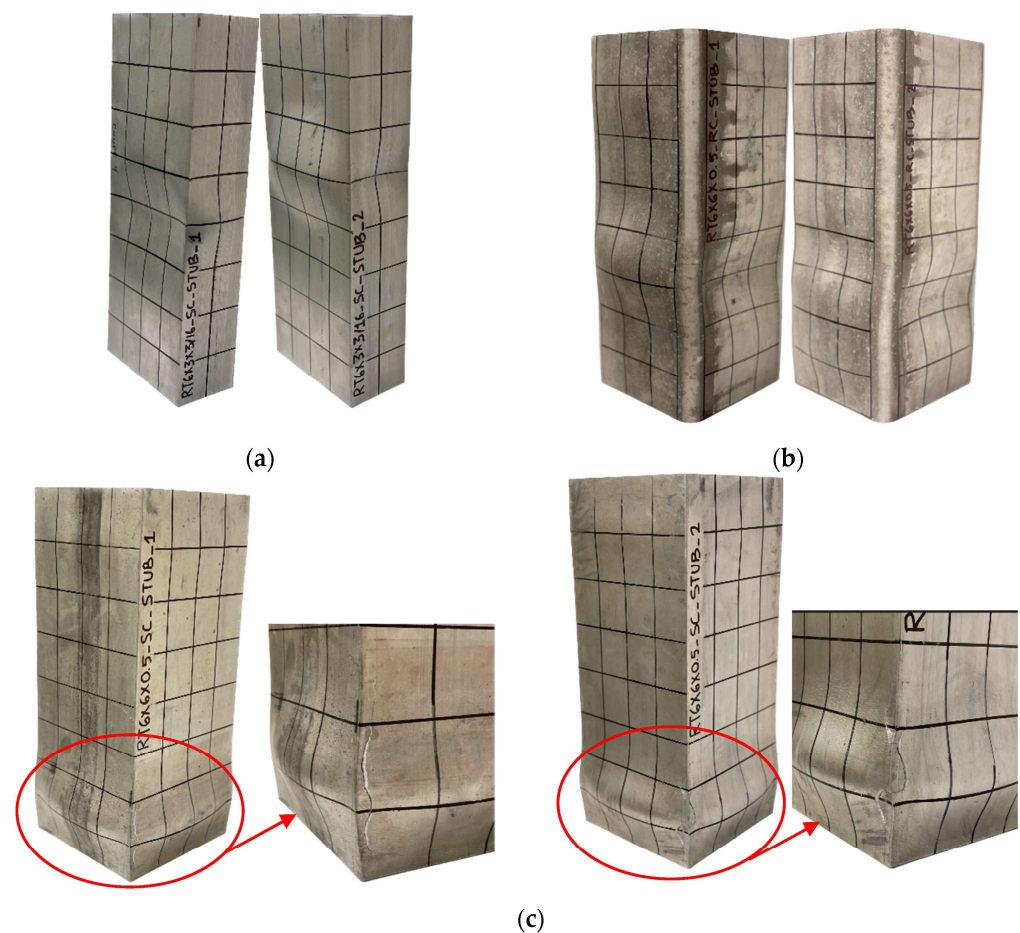


**Figure 4.** Failure modes during the stub column tests in the case of (a) square hollow sections with sharp corners, (b) square hollow sections with rounded corners, and (c) rectangular hollow sections with sharp corners.

The key results from the stub column tests are summarized in Table 3 in terms of peak load  $N_{exp}$  and axial displacement  $\delta_{exp}$ . The predicted resistance of the sections by the Canadian design code CSA S157A is also reported in the table. It is important to note that for the predicted resistance values, the experimental dimensions and material law obtained from the laboratory measurements were utilized. This ensures that the predicted resistance values are based on the specific characteristics of the tested sections, providing more accurate results for comparison with the experimental data. The comparison between the measured and predicted resistances showed significant differences (a maximum difference of 38%) between these two resistances, with the measured values being always conservative. Such differences between the experimental and design predictions are mostly due to the fact that the provisions of the CSA S157 neglect the significant strain-hardening benefits of

aluminum alloys, which significantly increased the experimental resistance of the sections under compression.

**Table 3.** Stub column test results.

Sections	$\delta$ [mm]	$N_{exp}$ [kN]	$N_{CSA-S157}$ [kN]	$N_{exp}/N_{CSA-S157}$ [-]
RT6 × 6 × 0.5-SC-STUB-1	17.80	2403.05	1918.4	1.25
RT6 × 6 × 0.5-SC-STUB-2	17.30	2200.8	1873.8	1.17
RT6 × 6 × 0.5-RC-STUB-1	20.10	2439.30	1769.6	1.38
RT6 × 6 × 0.5-RC-STUB-2	10.35	2440.80	1781.0	1.37
RT6 × 3 × 3/16-SC-STUB-1	2.25	529.40	455.5	1.16
RT6 × 3 × 3/16-SC-STUB-2	5.80	522.90	454.8	1.15

#### 4. Ongoing Short Beam-Column Tests

Currently, a series of 11 short beam-column tests under eccentric compression are being conducted to study the local buckling response of specimens subjected to combined compression and bending, including both uniaxial and biaxial bending loading conditions. These tests are performed on an MTS 2000 kN hydraulic testing machine with displacement control. Pin-ended configurations are implemented at both ends of the specimens using a cylindrical hinge device. This setup allows accurate replication of the structural response under combined compression and bending. The results from these ongoing tests will provide valuable insights into the local buckling behavior and the effects of combined loading on the specimens.

#### 5. Conclusions and Future Works

The main focus of this study was to investigate the buckling behavior of aluminum extrusions, which will eventually be used to improve the current design rules for aluminum structural members under axial compression and combined loading conditions. The scope of this study specifically focused on six 6061-T6 aluminum alloy extrusions featuring rectangular and square hollow sections. To ensure accurate data collection for further analysis, the geometrical properties of the specimens, including the dimensions and geometrical imperfections, were meticulously measured using a combination of mechanical techniques and advanced 3D scanning technologies. In addition, material properties were determined through classical tensile coupon tests. All these measured geometrical and material properties will contribute towards validating the numerical models that will be developed to further extend the current investigation to numerical environment.

The results from the stub column tests show significant differences between the experimental results and those predicted by the Canadian design code CSA S157. This is mostly due to the fact that the design predictions do not take into account the substantial strain-hardening effects associated with aluminum alloys. These strain-hardening effects have the potential to significantly increase the capacity of the sections, especially for compact shapes. As a result, accounting for these additional capacities can lead to significant design cost reductions, positioning aluminum as a competitive alternative to conventional structural materials.

As the tests under compression and bending are ongoing, a thorough evaluation of the results is not yet available. However, based on the preliminary studies, it is evident that there is a clear need to develop improved design models for the buckling of aluminum extrusions. To achieve this, a nonlinear finite element analysis will be performed on the aluminum sections using ABAQUS software to develop numerical models that will be further validated using the experimental results. These numerical models will provide a comprehensive understanding of the buckling behavior of aluminum extrusions. Finally, based on the observations from the experimental and numerical studies, the current design provisions will be evaluated and, subsequently, an innovative buckling design approach will be developed based on the principles of the Overall Interaction Concept (O.I.C.).

**Author Contributions:** Conceptualization, S.D., N.B. and P.D.; methodology, S.D., N.B. and P.D.; formal analysis, S.D.; investigation, S.D.; resources, L.L., S.D. and P.V.; data curation, S.D.; writing—original draft preparation, S.D.; writing—review and editing, S.D., P.D. and N.B.; visualization, S.D.; supervision, N.B. and P.D.; project administration, P.D. and N.B.; funding acquisition, P.D. and N.B. All authors have read and agreed to the published version of the manuscript.

**Funding:** This research was funded by Fonds de recherche du Québec (FRQNT)—FT131760.

**Institutional Review Board Statement:** Not applicable.

**Informed Consent Statement:** Not applicable.

**Data Availability Statement:** The data presented in this study are available on request from the corresponding author.

**Acknowledgments:** Special thanks to MAADI Group Inc. for providing the test specimens, to Denis Ouellet for his assistance in the scanner operations, and to Hugues Ferland for all the experimental investigations.

**Conflicts of Interest:** The authors declare no conflict of interest.

## References

1. Müller, U. *Introduction to Structural Aluminium Design*; Whittles Publishing: Dunbeath, UK, 2011; p. 194.
2. Dwight, J. *Aluminium Design and Construction*; CRC Press: London, UK; New York, NY, USA, 1999; p. 302.
3. Mazzolani, F. *Aluminium Structural Design*; Springer: New York, NY, USA, 2002; p. 398.
4. Mennink, J. *Cross-Sectional Stability of Aluminium Extrusions*. Ph.D. Thesis, Technische Universiteit Eindhoven, Eindhoven, The Netherlands, 2003.
5. Abdullah, K.A.; Mohamed Ali, J.S.; Aminanda, Y. Experimental and Numerical Simulation of Hollow Structure under Compression Loading. *AMR* **2012**, *576*, 651–654. [[CrossRef](#)]
6. Faella, C.; Mazzolani, F.M.; Piluso, V.; Rizzano, G. Local Buckling of Aluminum Members: Testing and Classification. *J. Struct. Eng.* **2000**, *126*, 353–360. [[CrossRef](#)]
7. Su, M.; Young, B.; Gardner, L. Testing and Design of Aluminum Alloy Cross Sections in Compression. *J. Struct. Eng.* **2014**, *140*, 04014047. [[CrossRef](#)]
8. Su, M.; Young, B.; Gardner, L. Deformation-Based Design of Aluminium Alloy Beams. *Eng. Struct.* **2014**, *80*, 339–349. [[CrossRef](#)]
9. Feng, R.; Liu, J. Numerical Investigation and Design of Perforated Aluminium Alloy SHS and RHS Columns. *Eng. Struct.* **2019**, *199*, 109591. [[CrossRef](#)]
10. Zhu, J.-H.; Young, B. Tests and Design of Aluminum Alloy Compression Members. *J. Struct. Eng.* **2006**, *132*, 1096–1107. [[CrossRef](#)]
11. Zhou, F.; Young, B.; Zhao, X.-L. Tests and Design of Aluminum Tubular Sections Subjected to Concentrated Bearing Load. *J. Struct. Eng.* **2009**, *135*, 806–817. [[CrossRef](#)]
12. Feng, R.; Zhu, W.; Wan, H.; Chen, A.; Chen, Y. Tests of Perforated Aluminium Alloy SHSs and RHSs under Axial Compression. *Thin-Walled Struct.* **2018**, *130*, 194–212. [[CrossRef](#)]
13. Mazzolani, F.M.; Piluso, V.; Rizzano, G. Local Buckling of Aluminum Alloy Angles under Uniform Compression. *J. Struct. Eng.* **2011**, *137*, 173–184. [[CrossRef](#)]
14. Wang, Z.; Wang, Y.; Yun, X.; Gardner, L.; Hu, X. Experimental and Numerical Study of Fixed-Ended High-Strength Aluminum Alloy Angle-Section Columns. *J. Struct. Eng.* **2020**, *146*, 04020206. [[CrossRef](#)]
15. Adeoti, G.O.; Fan, F.; Wang, Y.; Zhai, X. Stability of 6082-T6 Aluminium Alloy Columns with H-Section and Rectangular Hollow Sections. *Thin-Walled Struct.* **2015**, *89*, 1–16. [[CrossRef](#)]
16. Zhu, J.-H.; Young, B. Experimental Investigation of Aluminum Alloy Thin-Walled Tubular Members in Combined Compression and Bending. *J. Struct. Eng.* **2006**, *132*, 1955–1966. [[CrossRef](#)]
17. Creaform. Discover the Best Measuring Arm. Yours. [Online]. Available online: <https://www.creaform3d.com/en/optical-3d-scanner-metrascan> (accessed on 23 February 2023).
18. *B07 Committee*; Test Methods for Tension Testing Wrought and Cast Aluminum- and Magnesium-Alloy Products (Metric). ASTM International: West Conshohocken, PA, USA, 2023.
19. *European Standard EN ISO 377*; Steel and Steel Products—Location and Preparation of Samples and Test Pieces for Mechanical Testing. European Standards: Pilsen, Czech Republic, 1997.
20. Huang, Y.; Young, B. The Art of Cold-Formed Steel and Aluminium Alloy Coupon Tests. In Proceedings of the 7th European Conference on Steel and Composite Structures, Naples, Italy, 10–12 September 2014.

**Disclaimer/Publisher’s Note:** The statements, opinions and data contained in all publications are solely those of the individual author(s) and contributor(s) and not of MDPI and/or the editor(s). MDPI and/or the editor(s) disclaim responsibility for any injury to people or property resulting from any ideas, methods, instructions or products referred to in the content.